Correction of Movement Artifacts from 4-D Cardiac Short- and Long-Axis MR Data

Jyrki Lötjönen[1], Mika Pollari[2], Sari Kivistö[3], and Kirsi Lauerma[3]

[1] VTT Information Technology, P.O.B. 1206, FIN-33101 Tampere, Finland
{Jyrki.Lotjonen@vtt.fi}
[2] Laboratory of Biomedical Engineering, Helsinki University of Technology, P.O.B. 2200, FIN-02015 HUT, Finland
[3] Helsinki Medical Imaging Center, Helsinki University, P.O.B. 281, FIN-00029 HUS, Finland

Abstract. Typically a cardiac MR cine series consists of images over several time points but only from one spatial location. The volumetric information is obtained by combining 2-D slices from different image series. If a patient moves during an MR imaging session, the slices from different image series shift relative to each other, and the 3-D volume reconstructed does not represent the real geometry. In this study, an algorithm was developed to correct movement artifacts simultaneously from short- and long-axis MR cine series. The performance of the algorithm was evaluated by calculating the accuracy of the method against simulated movements imposed on real data, and by visually inspecting the results with real patient images. In both cases, the algorithm reduced significantly movement artifacts.

1 Introduction

Because cardiovascular disease is the most common cause of death in the Western countries, there is a strong need to diagnose and to quantify cardiac diseases. Magnetic resonance (MR) imaging provides detailed anatomical and functional information on the heart. Usually the structures of interest need to be segmented before volumetric measures, such as the ejection fraction, can be computed from the images. As the cardiac function is studied, the segmentation must be performed to images from various phases of the cardiac cycle. Therefore, there have been intense development efforts for automated analysis of the cardiac images during the last years [1]. Several approaches have been proposed for the automated segmentation and volume tracking of the ventricles and myocardium from MR images [2,3,4,5,6].

The use of 3-D data in segmentation is not straightforward because of movement artifacts. Typically, several MR image series are acquired during one imaging session. If a subject moves during an imaging session, the relation between the image series, derived from image headers, is lost and image registration is needed to realign the images. A subject may move because of several reasons, e.g. coughing, breathing or change of inconvenient pose. Breathing is a major source of movement artifacts in cardiac imaging, as the movement due to the heart beating is handled by the ECG gating. McLeish et al. [7] studied the movements of the heart due to respiration. They observed translations up to 23.5 mm in the heart because of breathing. When the cine sequences are used to track the cardiac motion, an image series produced during a breath hold typically contains

C. Barillot, D.R. Haynor, and P. Hellier (Eds.): MICCAI 2004, LNCS 3217, pp. 405–412, 2004.

slices from several time points but only from one spatial location. If the phase of the breathing cycle is not similar during all acquisitions, slices from different image series will be misaligned relative to each other, and a volume built from the image series does not represent the real anatomy of the subject. Although future scanner generations with faster speeds, e.g. fast sampling of k-space using kt-blast, the problem of movement correction is currently relevant in many clinical centers.

The problem has been discussed and reported very little in the literature. Moore et al. [8] recently built a high resolution dynamic heart model from coronal slices acquired from a healthy volunteer. They corrected the breath-hold misalignment by registering a 3-D volume with sagittal and axial scout images. A line-by-line mean squared difference was minimized. In this work, we extended this idea to the registration of two volumes. We optimize the locations of short-axis (SA) slices based on data from long-axis (LA) slices and vice versa. In this work, the movement artifacts are corrected only by translations although the respiration cause also small (typically a couple of degrees) rotations to the heart [7].

2 Methods

2.1 Transformation Between Short- and Long-Axis Images

Since both SA and LA slices are utilized in the movement correction, voxel-by-voxel based correspondence needs to be defined between the image volumes. In the following, the co-ordinates of a voxel in the source volume, denoted by (X, Y, Z), are defined in the co-ordinate system of the destination volume, denoted by (X', Y', Z'). The co-ordinate system of the imaging device is denoted by (X^*, Y^*, Z^*). Next, the parameters for the source volume are defined. Corresponding symbols for the destination volume have a dash. The voxel size of the source volume is (s_x, s_y, s_z). The voxel size in the z-direction is defined to be the distance between neighboring slices, i.e. slice separation. The position of the first voxel of the source volume in the scanner's co-ordinate system is denoted by (o_x, o_y, o_z). In addition, the orientation of x- and y-directions (row and column) are denoted by (r_x, r_y, r_z) and (c_x, c_y, c_z). The normal vector (n_x, n_y, n_z) of the slices can be computed, for example, by subtracting the image positions of the second and the first slices of the volume, and normalizing its length.

The location of a source voxel in the co-ordinate system of a scanner is computed as follows:

$$X^* = s_x X r_x + s_y Y c_x + s_z Z n_x + o_x \quad (1)$$

$$Y^* = s_x X r_y + s_y Y c_y + s_z Z n_y + o_y \quad (2)$$

$$Z^* = s_x X r_z + s_y Y c_z + s_z Z n_z + o_z. \quad (3)$$

The location of the voxel in the co-ordinate system of the destination volume is computed as follows:

$$X' = [(X^* - o'_x)r'_x + (Y^* - o'_y)r'_y + (Z^* - o'_z)r'_z]/s'_x \quad (4)$$

$$Y' = [(X^* - o'_x)c'_x + (Y^* - o'_y)c'_y + (Z^* - o'_z)c'_z]/s'_y \quad (5)$$
$$Z' = [(X^* - o'_x)n'_x + (Y^* - o'_y)n'_y + (Z^* - o'_z)n'_z]/s'_z. \quad (6)$$

2.2 Movement Correction

The movement artifacts can be visually observed by forming an image volume from cine series and computing a cross-section of the volume. Fig. 1a shows one original SA and LA slice from a subject having severe movement artifacts. The horizontal lines superimposed on the images indicate the cross-section planes. The cross-sections computed from the SA (six slices) and LA volumes (eight slices) are shown below the original slices. The cross-sections have been interpolated to isotropic voxel size using nearest neighbor interpolation for better visualizing the shifts. The dark, almost vertical stripe in the middle of the images represents the septum, which is normally a smooth and continuous object.

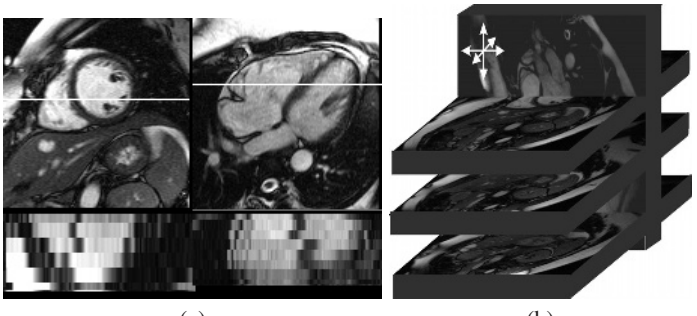

(a) (b)

Fig. 1. Movement correction. a) The top row shows original SA and LA slices. The horizontal lines represent the location of cross-sections, which are shown on the bottom row. b) The optimization of a LA slice relative to a SA volume. The arrows visualize the degrees of freedom for the movement correction.

The criterium of the smooth and continuous septum could be used to displace the slices in the SA and LA volumes separately. The problem in making the corrections separately is that the comprehensive shape information available in the other volume is not used. In other words, mapping the structures from the SA volume to the LA volume, using Eqs. $1-6$, could be inaccurate although the shape of the heart may appear to be realistic visually in both volumes separately.

To solve the problem, the normalized mutual information (NMI) [9], denoted by S, is maximized between the 4-D data

$$S(SA, LA) = \frac{H(SA) + H(LA)}{H(SA, LA)}, \quad (7)$$

where $H(SA)$ and $H(LA)$ are marginal entropies and $H(SA, LA)$ a joint entropy of the data. The voxel-by-voxel correspondence is calculated as described in Section 2.1.

Because all time points related to one spatial location have been acquired during the same breath-hold, data from all time instants can be used to compute the NMI. In other words, the whole image series is displaced simultaneously. The displacement of each image series is assumed to be independent on the displacements of the other image series. The step of displacement at each iteration corresponds to the voxel size in xy-plane (1.4 mm) by default. The basic idea of the registration algorithm is presented in Fig. 1b. Three methods were tested to maximize the NMI:

Gradient maximization. The slices of the two volumes are moved in the direction of an NMI gradient. The gradient of the NMI is computed as follows:

$$\nabla S = \sum_{i}^{N} \left(\frac{\partial S}{\partial \mathbf{r}_i}\mathbf{e}_{\mathbf{r_i}} + \frac{\partial S}{\partial \mathbf{c}_i}\mathbf{e}_{\mathbf{c_i}} + \frac{\partial S}{\partial \mathbf{n}_i}\mathbf{e}_{\mathbf{n_i}}\right) + \sum_{i}^{N'} \left(\frac{\partial S}{\partial \mathbf{r'}_i}\mathbf{e}_{\mathbf{r'_i}} + \frac{\partial S}{\partial \mathbf{c'}_i}\mathbf{e}_{\mathbf{c'_i}} + \frac{\partial S}{\partial \mathbf{n'}_i}\mathbf{e}_{\mathbf{n'_i}}\right), \quad (8)$$

where N and N' denote the number of slices in the SA and LA volumes, respectively, $\mathbf{r}_i$, $\mathbf{c}_i$ and $\mathbf{n}_i$ are the row, column and normal vectors of the SA slice i (see Section 2.1), and $\mathbf{e}$ denotes a basis vector. All row, column and normal vectors within a volume are equal but the index is used to indicate for which slice the gradient is computed (all slices are moved independently).

Random volume maximization. A slice is chosen randomly and moved in the direction of its gradient. The NMI of the volumes is maximized.

Random slice maximization. As *Random volume* maximization, but the NMI of the slice chosen and the other volume is maximized.

The slice locations are iterated until the NMI does not increase more than a user-defined parameter ϵ ($\epsilon = 0.0001$ in this study).

The displacements in x- and y-directions can be easily applied to the stack of slices. The displacements in z-direction change the slice separation which can be seen only after interpolating the data to isotropic voxel size.

2.3 Materials and Evaluation Protocol

The algorithm was developed for correcting the datasets scanned using a 1.5 T Siemens Magnetom Vision and Siemens Sonata imagers (Siemens, Erlangen, Germany) at the Helsinki Medical Imaging Center, University of Helsinki. A standard imaging protocol adopted for cardiac patients in our unit is following: SA images contain ventricles from valve level until the level where the apex is still visible, and LA images contain atria and ventricles. Temporal resolution of 30-40 ms results in 22-30 time points of cardiac cycle, depending on the heart rate of the subject. The pixel size is 1.4×1.4 mm and the slice thickness is 7 mm for the SA and LA images. The corresponding values for the slice separation are 15 mm and 10 mm. The number of SA and LA slices is $4-6$ and $4-8$ depending on the size of the heart.

The datasets described above can not be used to evaluate the performance of the algorithm because the ground-truth, i.e. movements during the acquisition, is not known. Therefore, we chose a following protocol: 1) We acquired a T1-weighted SA dataset including the atria and ventricles. The pixel size was 1.4×1.4 mm, the slice separation 10 mm and the number of time points 10. No movement artifacts were detected visually. 2) The data were interpolated to isotropic voxel size using shape-based interpolation [10].

3) MR imaging was simulated and a new set of SA and LA slices was generated from the volume using the image parameters (pixel size, gap, slice thickness) of our standard imaging protocol. Although the original SA slices may contain some movement artifacts, the simulated volumes do not include any movement artifacts relative to the original volume. 4) All SA and LA slices were randomly translated in x-, y- and z-directions. The displacements were chosen from an uniform distribution between $[-7.5, 7.5]$ mm in each direction. 5) The correction algorithm was applied and the movements of each slice were compared to the simulated movements. The registration error was defined as follows:

$$e = \frac{\sum_i^N \|\mathbf{s}_i + \mathbf{d}_i\| + \sum_i^{N'} \|\mathbf{s}'_i + \mathbf{d}'_i\|}{N + N'} \tag{9}$$

where $\mathbf{s}_i$ and $\mathbf{d}_i$ are the simulated movement and the correction, respectively, of the SA slice i, and N is the number of the SA slices. The dashed symbols represent corresponding parameters for the LA slices. 6) The steps 4 and 5 were repeated 50 times to evaluate the robustness of the algorithm.

3 Results

Fig. 2a contains the averaged registration errors ($N = 50$) for the simulated SA and LA volumes. The results are shown for the gradient and random maximization techniques, as displacement are allowed either in xy- or xyz-directions of each slice. The root mean square (RMS) and mean errors were computed. In addition, the slice with the maximum error after registration was detected, and a mean ($N = 50$) was defined. Random slice maximization technique computed for all three orientations produced the best results. The difference was statistically significant (paired T-test) as compared with the gradient ($p < 0.00001$) and random volume maximization ($p < 0.01$) techniques.

	RMS	Mean	Mean of max
No correction	6,95	6,6	10,42
Gradient, xy	4,52	3,94	8,37
Gradient, xyz	1,17	0,94	2,76
Random volume, xy	4,64	4,02	8,8
Random volume, xyz	0,85	0,74	1,78
Random slice, xy	4,67	4,04	8,82
Random slice, xyz	0,69	0,64	1,17
Best combination	0,54	0,49	0,89

(a)

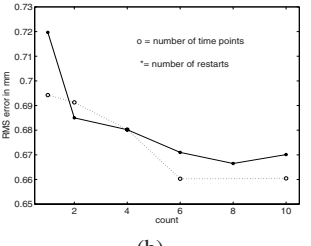

(b)

Fig. 2. a) Registration errors (in [mm]) computed over 50 simulated movements for different parameter combinations. b) The registration error in function of number of time points and restarts as the random slice minimization technique was used.

Several parameter combinations were tested:

The step size of the displacements. The best results were achieved as the registration was iterated first by the step size of one voxel (1.4 mm) and then by the step size of half voxel. Reducing the step size more did not improve the accuracy anymore.

The number of time points. Our hypothesis was that the best results are obtained if all time points are used in registration. However, we noticed that similar accuracy was achieved already with six time points (Fig. 2b).

The number of restarts. If the number of the slices in the SA and LA volumes is altogether 12 and the location of each slice is optimized in all three directions, (x, y, z), the NMI-measure is a function of 36 parameters. Since the function is non-convex containing several local minima, the chosen path from the initial slice configuration to the slice configuration maximizing the NMI has an effect on the result. Because the random maximization technique is a stochastic process, the path is, in practice, different each time the program is run. Therefore, the program can be restarted several times and the path producing the maximum NMI is chosen. We noticed that the RMS error did not decrease considerably after a few restarts (Fig. 2b). The error even increased using ten restarts due to the stochastic variation.

The row *Best combination* presents results for the optimal parameter combination as the random slice minimization technique was used: the step sizes 1.4 and 0.7 mm, six time points and eight restarts were used. Otherwise, the following parameter combinations were used: the step size 1.4 mm, all time points and one restart.

In addition, the algorithm was applied to real patient data. Fig. 3 shows the results from four subjects having severe movement artifacts. The SA and LA volumes are visualized using a chessboard visualization technique before the movement correction (the top row of each subimage) and after the movement correction (the bottom row of each subimage). The first column of each subimage shows the volumes as the LA volume was transformed to the SA co-ordinate system. The second column visualizes the result as the SA volume was transformed to the co-ordinate system of the LA volume. As can be noticed from the images, the edges are more continuous across the chess-boxes with the movement correction than without it. The black boxes indicate that no data is available for that location in the volume, for example, the SA volume does not contain any data from atria. In Fig. 3c, the misalignment corresponds to about 15 mm.

4 Discussion

A novel algorithm was developed for correcting movement artifacts from cardiac short- and long-axis MR images. We applied the algorithm to about 30 data sets. In practice, a subject can normally keep almost an equal breathing phase between the acquisitions and no clear misalignment can be visually detected from the volumes in most cases. However, when movement artifacts existed, the automatic correction performed well. A good indication of successful movement correction was that as we segmented the images after the movement correction, the result (triangulated 3-D surface) fitted well to both SA and LA volumes. The movement correction is a pre-requisite if information from SA and LA images is combined for segmentation and tracking purposes [6].

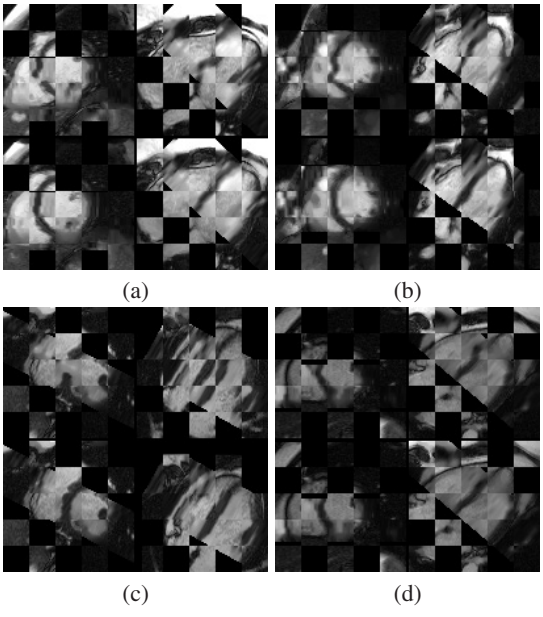

Fig. 3. Movement correction results for four cases (a,b,c and d) having severe movement artifacts. The chessboard visualization technique was used. The top and bottom rows of each subimage show the SA and LA data before and after, respectively, the movement correction. The left and right columns of each subimage show the data (SA and LA volumes) in the SA and LA co-ordinates systems, respectively.

Image series may contain slices which do not contain any or only small region of the heart, for example, the first or the last slice of the LA volume, or the most apical slice of the SA volume. We found that the algorithm fails often with these slices and produce incorrect results because the slices do not contain enough image features for registration. However, we did not try to develop any automatic method to detect these slices and leave them out from the registration. The movement correction is only a necessary preprocessing step for segmentation of the heart from the volumes. If the slices do not contain data from the heart, they also do not cause problems to segmentation.

The manual correction of the movement artifacts based on visual inspection is relatively time consuming and also very difficult. Although making different cross-sections from the volumes helps considerably the manual correction, often the result is still open to interpretations. The definition of the movements in the z-direction, the direction perpendicular to the slice, was found important in our study but it is almost impossible to obtain it manually in practice. In addition, making manually corrections which produce the similar 3-D geometry in the both volumes, is neither an easy task. For these reasons, an automatic method was needed. The algorithm developed makes the corrections in a few seconds, and it has proved to be robust also to large artifacts.

Acknowledgements. This research was supported by the National Technology Agency, Finland. This study was partly financed by a grant from Helsinki University Central Hospital Research Fund (T181032, TYH 2242), the Radiology Society of Finland, Pehr Oscar Klingendahl Foundation, BIOMEDICUM Helsinki Foundation, the Graduate School "Functional Research in Medicine" (Academy of Finland, Ministry of Education), Waldemar von Frenckell Foundation.

References

1. Frangi, A., Niessen, W., Viergever, M.: Three-dimensional modeling for functional analysis of cardiac images: A review. IEEE Trans. Med. Imag. **20** (2001) 2–25
2. Jolly, M.P.: Combining edge, region, shape information to segment the left ventricle in cardiac MR images. In Niessen, W.J., Viergever, M.A., eds.: Lecture Notes in Computer Science 2208: Medical Image Computing and Computer-Assisted Intervention - MICCAI 2001, Springer (2001) 482–490
3. Mitchell, S., Bosch, J., Lelieveldt, B., van der Geest, R., Reiber, J., Sonka, M.: 3-D active appearance models: Segmentation of cardiac MR and ultrasound images. IEEE Trans. Med. Imag. **21** (2002) 1167–1178
4. Lorenzo-Valdés, M., Sancheez-Ortiz, G., Mohiaddin, R., Rueckert, D.: Atlas-based segmentation and tracking of 3D cardiac MR images using non-rigid registration. In Dohi, D., Kikinis, R., eds.: Lecture Notes in Computer Science 2488: Medical Image Computing and Computer-Assisted Intervention - MICCAI 2002, Springer (2002) 642–650
5. Kaus, M., von Berg, J., Niessen, W., Pekar, V.: Automated segmentation of the left ventricle in cardiac MRI. In Ellis, R., Peters, T., eds.: Lecture Notes in Computer Science 2878: Medical Image Computing and Computer-Assisted Intervention - MICCAI 2003, Springer (2003) 432–439
6. Lötjönen, J., Smutek, D., Kivistö, S., Lauerma, K.: Tracking atria and ventricles simultaneously from cardiac short- and long-axis MR images. In Ellis, R., Peters, T., eds.: Lecture Notes in Computer Science 2878: Medical Image Computing and Computer-Assisted Intervention - MICCAI 2003, Springer (2003) 440–450
7. McLeish, K., Hill, D., Atkinson, D., Blackall, J., Razavi, R.: A study of the motion and deformation of the heart due to respiration. IEEE Trans. Med. Imag. **21** (2002) 1142–1150
8. Moore, J., Drangova, M., Wierzbicki, M., Barron, J., Peters, T.: A high resolution dynamic heart model based on averaged MRI data. In Ellis, R., Peters, T., eds.: Lecture Notes in Computer Science 2878: Medical Image Computing and Computer-Assisted Intervention - MICCAI 2003, Springer (2003) 549–555
9. Studholme, C., Hill, D., Hawkes, D.: Automated three-dimensional registration of magnetic resonance and positron emission tomography brain images by multiresolution optimization of voxel similarity measures. Medical Physics **24** (1997) 71—86
10. Grevera, G.J., Udupa, J.K.: Shape-based interpolation of multidimensional grey-level images. IEEE Trans. Med. Imag. **15** (1996) 881–892
11. Lötjönen, J., Mäkelä, T.: Elastic matching using a deformation sphere. In Niessen, W.J., Viergever, M.A., eds.: Lecture Notes in Computer Science 2208: Medical Image Computing and Computer-Assisted Intervention - MICCAI 2001, Springer (2001) 541–548